FC

Department of the Navy
Office of Naval Research
Contract N6onr-24424
Project NR 234-001

FLOW AROUND BODIES WITH ATTACHED OPEN CAVITIES

J. P. O'Neill

Hydrodynamics Laboratory
California Institute of Technology
Pasadena, California

Report No. E-24.7

December 1954

Department of the Navy
Office of Naval Research
Contract N6onr-24424
Project NR 234-001

FLOW AROUND BODIES WITH ATTACHED OPEN CAVITIES

J. P. O'Neill

Hydrodynamics Laboratory
California Institute of Technology
Pasadena, California

Report No. E-24.7

December 1954

CONTENTS

SYMBOLS AND EQUATIONS

		Eq. No.	1st Text Reference Page
V_∞	Velocity of undisturbed flow.		1
p	Local pressure at any point.		1
C_p	Pressure coefficient		
	$C_p = \frac{p - p_\infty}{q}$	(1)	1
p_∞	Pressure in the undisturbed fluid.		2
q	Dynamic pressure		
	$q = \frac{1}{2} V_\infty^2$.		2
ρ	Density.		2
V	Velocity at any point in the flow.		2
C_p	Pressure coefficient		
	$C_p = \frac{p - p_\infty}{q} = 1 - \left(\frac{V}{V_\infty}\right)^2$	(2)	2
p_{st}	Stagnation pressure		
	$p_{st} = p_\infty + q$.		2
p	Local pressure at any point		
	$p = C_p\ q + p_\infty$.		2
p_v	Vapor pressure of the liquid .		2
σ_v	Vapor cavitation parameter		3
	$\sigma_v = \frac{p_\infty - p_v}{q}$.	(3)	3
σ_{vi}	Incipient vapor cavitation parameter.		3
p_k	P ressure in open cavity regardless of the gas with which the cavity space is filled.		5
σ_k	Cavity parameter		
	$\sigma_k = \frac{p_\infty - p_k}{q}$,	(4)	5
	the characteristic parameter for open cavities of any type, regardless of what gas fills the cavity at a pressure p_k .		

Symbols and Equations
(cont'd)

		Eq. No.	1st Text Reference Page
V_k	Velocity of the cavity boundary streamline,		5
	The Bernoulli equation		
	$$\frac{1}{2}\rho V_\infty^2 + p_\infty = \frac{1}{2}\rho V_k^2 + p_k$$	(5)	5
	reduces to the ratio		
	$$\frac{V_k^2}{V_\infty^2} = 1 + \sigma_k$$	(6)	5
	and determines the velocity of the cavity boundary streamline		
	$$V_k = V_\infty (1 + \sigma_k)^{1/2} .$$	(7)	6
C_D	Drag coefficient		
	$$C_D \equiv \frac{D}{qA_D} .$$	(8)	7
D	Drag force on the body in the flow.		7
A_D	Transverse area of the body at		7
d	the diameter where the flow separates to form the cavity.		7
	The pressure across an elemental area of a body having an attached open cavity is		
	$$p - p_k = q(C_p + \sigma_k) .$$	(9)	11
	The "stagnation cup" having $C_p = 1$ over its entire inside bottom surface will then have a drag coefficient		
	$$C_D = 1(1 + \sigma_k).$$	(10)	11
C_{D0}	Drag coefficient at $\sigma_k = 0$. For the "stagnation cup", $C_{D0} = 1$ and it therefore complies exactly with the relation		
	$$C_D = C_{D0}(1 + \sigma_k)$$	(11)	11
	which holds approximately for any cavity-producing solid body.		

Symbols and Equations (cont'd)

		Eq. No.	1st Text Reference Page
V_j	Velocity of the re-entrant jet or the jet forming a jet cavity $V_j = V_\infty (1 + \sigma_k)^{1/2}$.		19
D_j	Drag of the jet cavity $D_j = Q\rho\Delta V$.	(12)	22
Q	Volume rate of flow of the jet liquid.		22
ΔV	Change in velocity of the jet liquid $\Delta V = V_\infty (1 + \sigma_k)^{1/2} + V_\infty$.		22
A_j	Transverse area of the jet.		22
D_j	Drag of the jet cavity $D_j = \rho A_j V_\infty^2 \left[(1 + \sigma_k) + (1 + \sigma_k)^{1/2}\right]$.	(13)	22
C_{Dj}	Drag coefficient of the jet cavity $C_{Dj} = \frac{D_j}{qA_j} = 2\left[(1 + \sigma_k) + (1 + \sigma_k)^{1/2}\right]$	(14)	22
	$\approx 4 + 3\,\sigma_k$.	(14')	22
C_D	Drag coefficient of any body producing a cavity, expressed in terms of the ratio of the area of the re-entrant jet to the area of the body, $C_D = 2\left[(1 + \sigma_k) + (1 + \sigma_k)^{1/2}\right] \frac{A_j}{A_D}$	(15)	22
	$\approx \frac{A_j}{A_D} (4 + 3\,\sigma_k)$.	(15')	23
	The area ratio is, therefore $\frac{A_j}{A_D} = \frac{C_D}{2\left[(1 + \sigma_k) + (1 + \sigma_k)^{1/2}\right]}$	(16)	23
	$\approx \frac{C_D}{4 + 3\,\sigma_k}$	(16')	23

Symbols and Equations
(cont'd)

		Eq. No.	1st Text Reference Page
or, by use of C_{D0},			
	$\frac{A_j}{A_D} = \frac{C_{D0}(1+\sigma_k)}{2\left[(1+\sigma_k)+(1+\sigma_k)^{1/2}\right]}$	(17)	23
	$\approx \frac{C_{D0}}{4}\left(1+\frac{1}{4}\sigma_k\right)$.	(17')	23
C_{Dm}	The cavity drag coefficient, based on the cavity diameter		
	$C_{Dm} \equiv \frac{D}{qA_m}$.	(18)	24
A_m	Transverse area of the cavity at		24
d_m	the maximum diameter of the cavity.		24
	From the definition equations for C_{Dm} and C_D,		
	$\sqrt{C_{Dm}} = \sqrt{C_D}\,\frac{d}{d_m}$.	(19)	24
ℓ	Length of cavity.		25

NOTE: All pressures denoted throughout the report are absolute.

Introduction

When a solid body is submerged in a liquid, its surfaces contact the liquid and remain in contact at low flow velocities. Very high velocities, however, may produce a condition in which only part of the surfaces contact the liquid. At some intermediate stage, the velocity will be just high enough to reduce the local pressure at some point on the body to the vapor pressure of the liquid, thus producing boiling or cavitation. In order to reach the vapor pressure, the amount of pressure reduction that must be brought about by the velocity of the liquid relative to the body depends on the ambient temperature and the submergence pressure.

At velocities considerably greater than that required for incipient cavitation, the liquid ceases to remain in contact with the entire surface of the body with the result that attached open vapor cavities are formed. The open cavity condition, however, does not require the cavity gas to be the liquid vapor. With another gas held at a pressure higher than the vapor pressure, the open cavity condition can be maintained at a more moderate velocity or a higher submergence.

The following analysis and summary of the characteristics of open cavities is based on part of an investigation of free-boundary flows conducted for the Office of Naval Research in the Free-Surface Water Tunnel at the Hydrodynamics Laboratory of the California Institute of Technology. The open cavity analysis is introduced by means of some considerations of noncavitating flow about a body, of the inception of vapor cavitation, and of the growth of open cavities.

The Pressure Coefficient

In an infinite extent of incompressible, nonviscous, noncavitating, steady flow having a uniform approach velocity V_∞ relative to a body in the flow, the local pressure p at various points in the vicinity of the body or on its furface can be given in terms of the dimensionless pressure coefficient

$$C_p = \frac{p - p_\infty}{q} \tag{1}$$

Here p_∞ is the pressure in the undisturbed fluid approaching the body and $q = 1/2\rho V_\infty^2$ is the dynamic pressure that can result from the relative motion of the fluid having a density ρ. The principal reason for introducing C_p is that its value at any point in such a flow field or on the boundaries is a function of only the body shape and orientation and is independent of the size of the body or of the values of ρ, V_∞, and p_∞.

The orientation of the body determines the point or points where the velocity is reduced to zero. Since the pressure p at any point having a velocity V can be compared with p_∞ where the velocity is V_∞ by means of the Bernoulli relationship

$$C_p = \frac{p - p_\infty}{q} = 1 - \left(\frac{V}{V_\infty}\right)^2 \qquad (2)$$

the pressure coefficient reaches its maximum value $C_p = 1$ at such a point of zero velocity and the corresponding pressure is the stagnation pressure $p_{st} = p_\infty + q$. The shape of the body then determines the velocity at other points on its boundary and in the flow field. In order for the fluid to pass around the obstacle, it is of course necessary that in some regions it be accelerated to local velocities higher than V_∞, and this results in negative values of the pressure coefficient and in local pressures that are lower than p_∞. The lowest value of the pressure coefficient, i.e., the negative term of greatest magnitude will occur somewhere on the surface of the body, as can be shown (see Lamb pp. 38-39). This might be expected since it is the presence of the body that causes the fluid to be accelerated to the higher velocities.

Vapor Cavitation

At the point where the pressure coefficient C_p is lowest, the local pressure $p = C_p q + p_\infty$ will be a minimum. A body with a sufficiently low value of C_p in a liquid flow of sufficiently high dynamic pressure q and low pressure p_∞ will cause the minimum local pressure p to be as low as the vapor pressure p_v. If we neglect boiling delay that requires a tension in the liquid, boiling or cavitation will occur at this low pressure point and produce cavities having an internal pressure p_v.

The flow can be described with respect to its potentialities for lowering p to p_v by using p_v in the dimensionless vapor cavitation parameter

$$\sigma_v = \frac{p_\infty - p_v}{q} \tag{3}$$

which is a function of the flow situation only, and independent of the body. This vapor cavitation parameter σ_v depends on the characteristics of the approaching flow; that is, the pressure p_∞, the vapor pressure p_v, and the dynamic pressure q which can result from the relative velocity V_∞. No reference to the effects of the shape of the body or boundaries under consideration is contained in σ_v; a low value of this parameter indicates only that the flow conditions have high potentialities for producing cavitation.

The cavitation situation for a particular body or boundary configuration is determined by comparing the vapor cavitation parameter σ_v for the flow conditions with the pressure coefficient C_p for the body. The comparison should be made with the lowest value of C_p that occurs on the body, since this determines the lowest pressure for a particular flow condition. When σ_v is as low as the maximum negative value of C_p, that is, when

$$\sigma_v = \sigma_{vi} = - C_p$$

or

$$\frac{p_\infty - p_v}{q} = \frac{p_\infty - p}{q},$$

then

$$p = p_v .$$

Except for boiling delay, cavitation will then be incipient.

Until σ_v is reduced to the critical value equal to the maximum negative value of C_p, it has no particular significance in determining the flow pattern about a body. This critical value of σ_v, i.e., σ_{vi}, however, is sometimes referred to as the "cavitation parameter" for the body shape. More specifically, it is the vapor cavitation parameter for the flow conditions that are critical for the body under consideration, in that they are just able to lower p to p_v at the point where C_p is lowest and thereby produce incipient cavitation. This σ_{vi} is the value of prime interest in hydraulic machinery and other applications where cavitation must be avoided.

Growth of Open Cavities

The vapor cavitation parameter σ_v, being a function of the flow conditions only, can be reduced below the critical value which produces incipient cavitation on a body. If there were still no alteration in the flow pattern, this would result in a region where the local pressure is less than p_v. With any chance rupture of the liquid in this region of tension, however, the flow pattern becomes dependent on the value of σ_v and the pressure will not be as low as $C_p q + p_\infty$. The simplified Bernoulli relationship does not apply when frequent rupture produces vapor cavitation bubbles that move along with the flow. The fluid is then no longer a homogeneous liquid of density ρ.

There might be any degree of relief of this tension in the liquid, depending on the history of the oncoming flow. This would be influenced by inertial effects governed by the time available for the radial growth of vapor bubbles, as well as by viscous and surface tension effects when real fluids are involved. Some of the studies in this laboratory have shown, for example, the large influence of the boundary layer on the time available for bubble growth. The minimum pressure might be expected to be no lower than p_v at any point on the boundary of the body where the oncoming flow was subjected to a sufficiently low pressure for a time adequate for the growth of closely-spaced vapor bubbles. The pressure should then increase monotonically from p_v at this point on the boundary to P_∞ far away along a line perpendicular to the flow direction, even though the values of C_p in this region for noncavitating conditions indicate lower pressures.

Another way for the pressure field to be altered from what is indicated by the values of C_p, obtained under noncavitating conditions, would be for the closely-spaced vapor bubbles to coalesce and become attached to the solid boundaries in the low-pressure region. In this case, the liquid is homogeneous but the boundary configuration for the liquid flow is altered. The open cavity will so alter the flow pattern that accelerations will not be of sufficient magnitude to produce velocities any higher than necessary for p to be reduced to p_v. The boundary configuration for the liquid flow then consists of an unalterable portion of the solid body followed by a free boundary that must assume some shape which produces the required local velocities. This total boundary shape must produce, as indicated by the flow net,

the pressure and velocity ratios that are necessary for the pressure to be p_v. Since these necessary ratios are determined by σ_v, it follows that the shape of the open vapor cavity is some function of σ_v.

With open cavities resulting from these low values of σ_v, it should be expected that any gas at the same pressure and having negligible dynamic effect could be substituted for the vapor without affecting the cavity shape. Furthermore, since the shape of the vapor cavity is a function of σ_v, in which the pressure difference $p_\infty - p_v$ is involved, the cavity shape should now depend on the difference between p_∞ and the pressure p_k in the new cavity gas without being affected by changing p_∞ and p_k by the same amount. With this gas pressure p_k substituted for the vapor cavity pressure p_v, the cavity parameter

$$\sigma_k = \frac{p_\infty - p_k}{q} \tag{4}$$

can be used as the characteristic parameter for open cavities of any type, regardless of what gas fills the cavity at a pressure p_k. Just as the shape of the open vapor cavity is a function of σ_v, the shape of an open cavity filled with any gas having negligible dynamic effect is a function of σ_k.

The lower the value of the cavity parameter σ_k, the nearer the velocity at the cavity wall V_k will be to the free-stream velocity. That the velocity ratio is near unity at low values of σ_k is shown by the Bernoulli equation

$$1/2\,\rho V_\infty^2 + p_\infty = 1/2\,\rho V_k^2 + p_k \tag{5}$$

for a stream filament adjacent to the cavity interface. Transposing and dividing by $q = 1/2\,\rho V_\infty^2$ gives

$$\frac{1/2\,\rho V_k^2}{1/2\,\rho V_\infty^2} = 1 + \frac{p_\infty - p_k}{1/2\,\rho V_\infty^2}$$

which reduces to the significant ratio

$$\frac{V_k^2}{V_\infty^2} = 1 + \sigma_k \tag{6}$$

and determines the velocity of the cavity boundary streamline

$$V_k = V_\infty (1 + \sigma_k)^{1/2} . \qquad (7)$$

Application of the flow net will show that a decreasing curvature of cavity wall is required when the ratio V_k^2/V_∞^2 is reduced toward unity by lowering σ_k. Since reduction of σ_k reduces the curvature of the free boundary, it causes the cavity to grow longer and attain a larger length-to-diameter ratio. Such long, slim cavities necessarily have small curvature over the major portion of their length. A change in this curvature by virtue of a change in σ_k, therefore has a marked influence on the cavity shape as described by the length-diameter ratio. The influence of the nose shape is confined principally to the end of the cavity, for otherwise a large portion of the length could not have the smooth contours that result from a low value of the cavity parameter. It seems, therefore, that the flow pattern soon becomes primarily a function of σ_k with the nose or front edge of the body contributing only minor local influences.

Cavity Theory and Measurement

It appears obvious that the size of an open cavity will be affected by the shape of the portion of the body in contact with the liquid. Since the gross geometrical configuration of the cavity and the pressure applied to the back side of the body is determined by the cavity parameter σ_k, the influence of the body shape is expected to be manifest in the pressure distribution over the wetted portion of the body and the resulting drag coefficient.

There have been theoretical determinations of many of these relations pertinent to flow about bodies with attached open cavities. Reichardt[1, 2] determined the dimensions and drag coefficients of axially symmetrical cavities as a function of the cavitation parameter by adjusting source-sink distributions to approach constant pressure at the boundary streamline. His computed values by such an approach were in close agreement with his extensive and systematic experimental measurements.

Plesset and Shaffer[3, 4, 5] have determined the dimensions, pressure coefficients, and drag coefficients for two-dimensional cavities formed behind wedges of various apex angles by numerically computing certain

integrals in terms of which these parameters can be represented. Perry[6] analytically re-evaluated some of the integrals and extended them for lower values of the cavity parameter. His evaluations of the drag and pressure coefficients and cavity dimensions were in agreement with the Plesset and Shaffer computations at high values of σ_k but resulted in some corrections to the cavity dimensions at low values of the cavity parameter.

Although theoretical computations for two-dimensional cavity flow configurations have been numerous, there have been few experimental measurements. Reichardt's measurements, often overlooked because they were presented in his report on axially symmetrical cavities[1], showed that the width of two-dimensional cavities produced by supporting a flat lamina in a free-jet tunnel were in reasonably close agreement with the computations. It has also been demonstrated by Perry that two-dimensional cavities can be produced in the Free-Surface Water Tunnel at the California Institute of Technology.

The sparsity of measurements on the two-dimensional configurations is possibly due to tunnel boundary effects being much more severe in this case than for axially symmetrical cavities. Reichardt's data, for example, showed some suggestion of boundary effects on the cavity dimensions when the width of the flat lamina was changed from 0.5 mm to 1.5 mm in a 20 cm free-jet tunnel. It therefore appears advisable that such measurements of the dimensions and pressure or drag coefficients of two-dimensional cavities be closely coordinated with evaluations of boundary effects.

By assuming that the distribution of the pressure coefficient from the apex to the edge of a cone is the same as for the two-dimensional wedge at the same value of σ_k, Plesset and Shaffer also computed the drag coefficients of cones at the head of axially symmetrical cavities. The drag coefficient is here defined as

$$C_D \equiv \frac{D}{q A_D} \tag{8}$$

where D is the drag force on the obstacle in the flow, A_D is its transverse area where the flow separates at the diameter d to form the cavity, and $q = 1/2\, \rho V_\infty^2$ as previously defined. In Fig. 1 is shown the agreement between these computed values of the drag coefficient of a disk and the

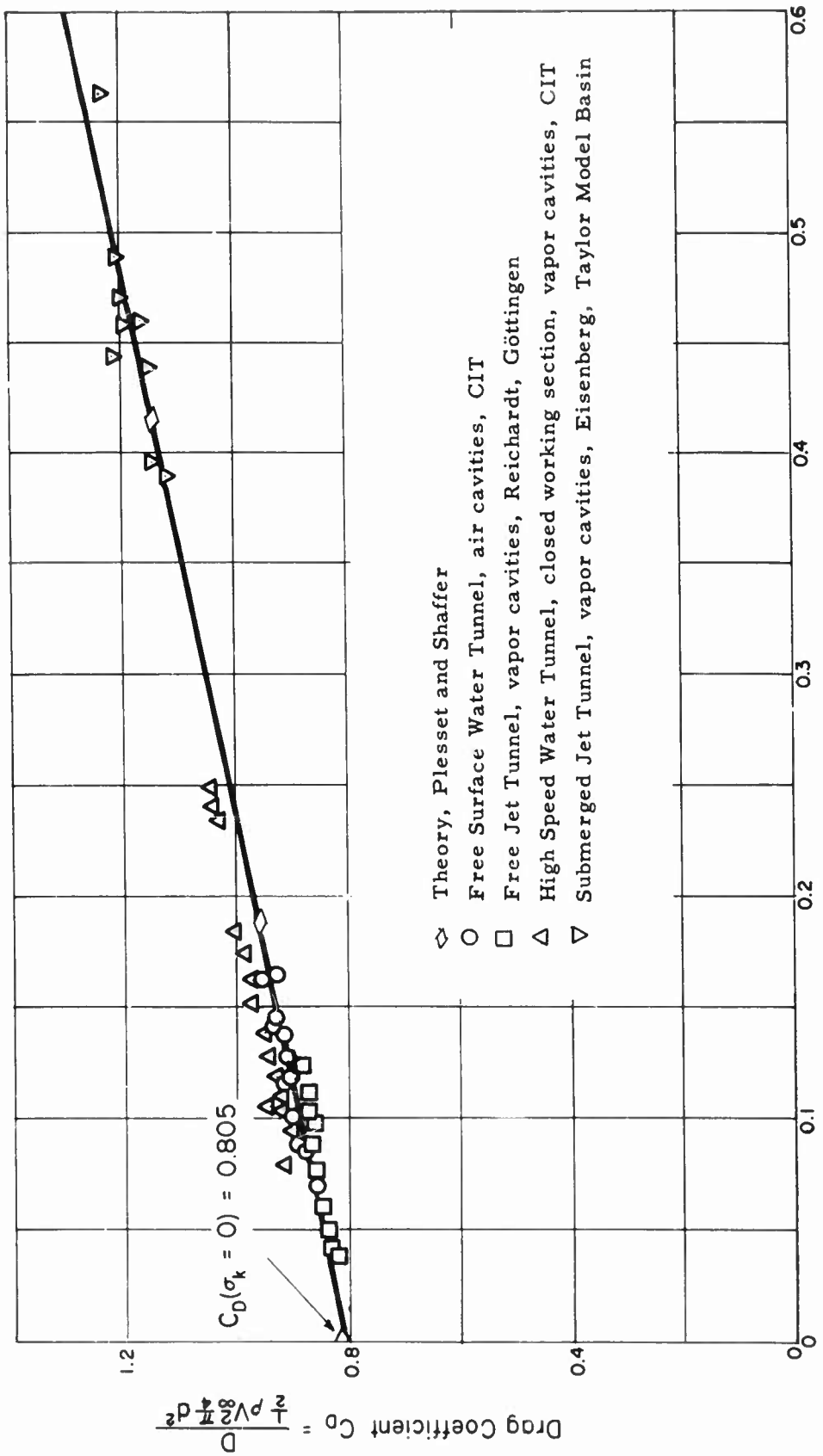

Fig. 1 - Drag coefficient vs. cavity parameter σ_k for the circular disk

experimental values over a very wide range of σ_k. The measurements were made on vapor cavities in a free-jet tunnel by Reichardt, on vapor cavities in a submerged-jet tunnel by Eisenberg[7], and in water tunnels of two different types at the California Institute of Technology where vapor cavities were used by Kermeen[8] in the High-Speed Water Tunnel which has a closed working section and air cavities were used in the Free-Surface Water Tunnel during the present investigation. It is seen that there is reasonably close agreement regardless of the type of tunnel boundary or of the gas which filled the cavity.

The cavity-drag measurements in the Free-Surface Water Tunnel, those by Kermeen in a closed working section, and those by Reichardt in a free-jet tunnel, were carried out for large variation in the bluffness of the head shape. The measurements were not extended to the higher values of σ_k because of difficulties with splash at the downstream end of the cavity. The nature of this re-entrant jet splash is discussed in more detail in later sections of this report. The measured values of the drag coefficient are compared with theory in Fig. 2. For the cones and disk, the theoretical curves are from the Plesset and Shaffer computations which were based on the assumption that the pressure distribution from the center to the edge of separation of the axially symmetrical shape is the same as that calculated for the corresponding two-dimensional shape. The theoretical curve for the cup assumes that its entire inside bottom surface is subjected to stagnation pressure.

Differences between the measured coefficients and the curves derived from two-dimensional theory might be expected. Even though the pressure coefficients are the same at the center and again at the separation edge, deviations might be expected at intermediate points. For some of the shapes, especially the slim cone of 15° half angle, there is also a difference between the slope of the theoretical curve and the plotted data that has not been satisfactorily explained. Although these differences may be due to some unknown experimental bias, it is interesting to note that for the cup there is good agreement with theory in both the slope and the values of the plotted data. This is the shape for which one might have the greatest confidence that two-dimensional theory is correct for the axially symmetrical case. This leads to consideration of the cup as a calibrating device for measurements of

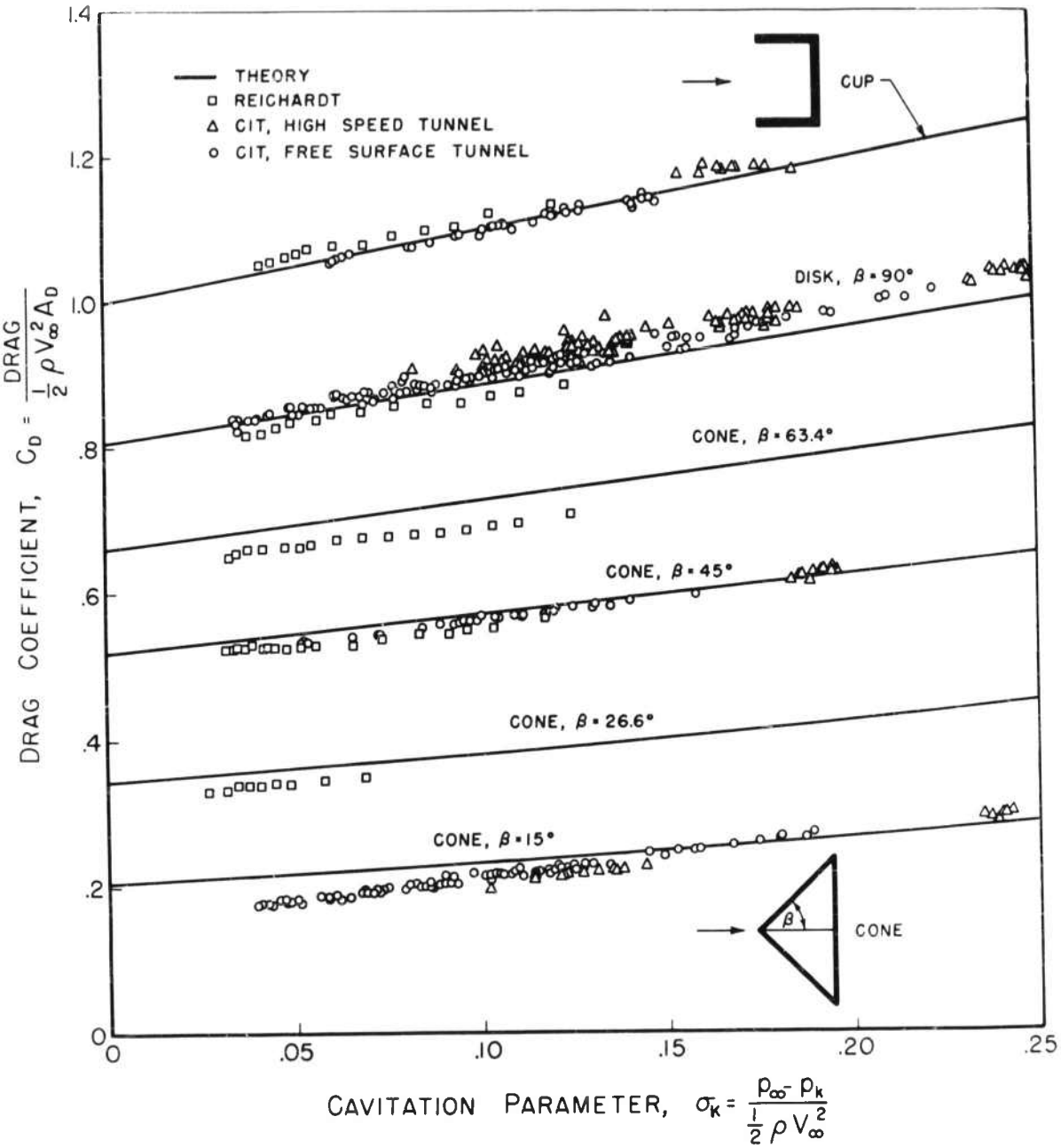

Fig. 2 - Drag coefficient vs. cavity parameter σ_k for cups, disks and cones

cavity drag.

Stagnation-Cup Flow

From Eqs. (1) and (4) it is seen that the pressure across an elemental area of a body having an attached open cavity is

$$p - p_k = q(C_p + \sigma_k). \tag{9}$$

The "stagnation cup" having $C_p = 1$ over its entire inside bottom surface will then have a drag

$$D = (p - p_k)A_D = qA_D(1 + \sigma_k)$$

and a drag coefficient

$$C_D = 1(1 + \sigma_k) . \tag{10}$$

At $\sigma_k = 0$, the drag coefficient $C_{D0} = 1$. The "stagnation cup", as here defined, therefore complies exactly with the relation

$$C_D = C_{D0}(1 + \sigma_k) \tag{11}$$

that has been shown by Reichardt, Plesset and Shaffer, and others to hold approximately for other head shapes at low values of σ_k. With adequate evaluation of the depth necessary to produce a stagnation cup within the accuracy of practical experimental measurements, the cup shows promise of providing an excellent calibrating device for water-tunnel and towing-tank measurements in cavity-running head shapes.

Some clue to the rapidity with which the drag coefficient of a cup approaches the value $1 + \sigma_k$ as the depth is increased, may be obtained from potential flow solutions for two-dimensional cup-shaped lamina. During the course of the present investigations, Perry[9] has calculated the pressure distribution across the bottom of cup-shaped two-dimensional lamina for various depth-width ratios. The results of these calculations shown in Fig. 3 indicate that only a small depth is necessary in order to approach very closely the "stagnation cup" having $C_D = 1$ over the entire bottom surface. When the depth is only 20% of the width, the drag coefficient of the two-dimensional lamina is already within 1/2% of its final value $C_{D0} = 1$ at $\sigma_k = 0$. Furthermore, it can be said with certainty that the cup-shaped lamina of moderate depth complies almost exactly with the relation

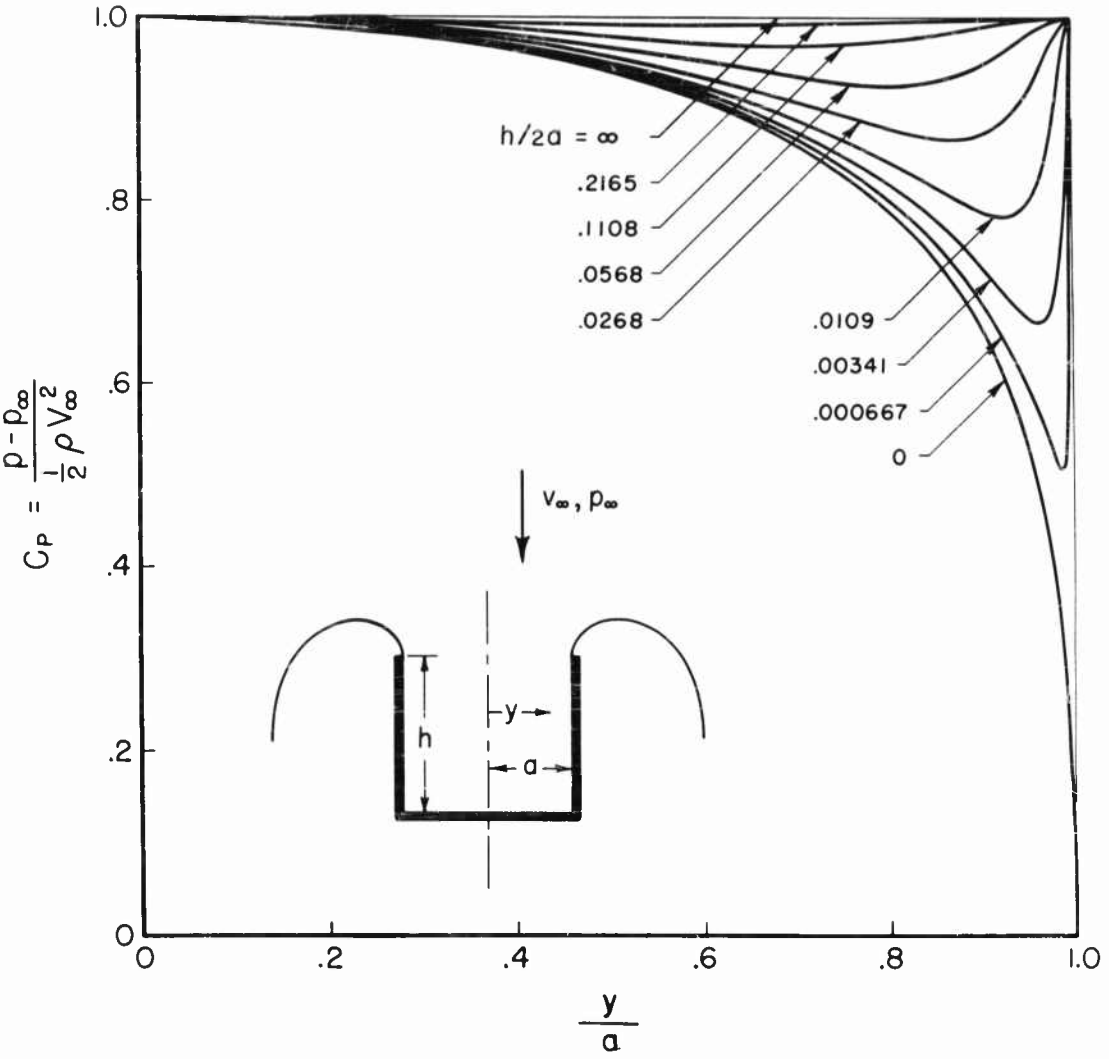

Fig. 3 - Pressure coefficients for the two-dimensional stagnation cup are shown as a function of the ratio of the distance y from the central stagnation line to the half-width a of the cup for various depth-width ratios.

$C_D = C_{D0}(1 + \sigma_k)$ expressed in Eq. (11) at low values of the cavity parameter. This is evident since it approaches the condition represented by Eqs. (10) and (11) exactly as the depth is increased, while even for zero depth, where it is identical with the flat lamina, the departure from Eq. (11) is only 0.2% at $\sigma_k = 0.42$.

By assuming that the pressure distributions of Fig. 3 hold for the axially symmetrical cup, the drag coefficient as a function of the depth-diameter ratio has been calculated. As shown in Fig. 4, the drag coefficient quickly approaches that of a stagnation cup, the deviation being less than 1/10 of one percent when the depth is equal to the radius. While it is often difficult to estimate even the direction of the error due to the application of two-dimensional theory to axially symmetrical flow configurations, it is believed that axially symmetrical cups of moderate depth have a true theoretical drag coefficient curve that is higher than that shown in Fig. 4 which is derived from two-dimensional pressure distributions. This hypothesis is based on the expectation that the side wall more effectively retards the flow proceeding away from the relatively small region about the central stagnation point of the axially symmetrical cup than that proceeding away from the larger region about the central stagnation line of the cup-shaped lamina.

It is concluded that the above or any more exact potential flow theory would require only a moderate depth for the drag coefficient to be practically as high as for the true stagnation cup. Since the velocities at the cup surfaces are lower than for any other shape, real fluid effects should cause the least deviation from theory. The stagnation cup should, therefore, make an excellent calibrating device for cavity measurements.

Stagnation-Cup Measurements

With the preceding hypothesis as an indication of the direction of the error in the three-dimensional theory due to its use of two-dimensional pressure distributions, it is inferred that only a small depth is necessary to produce a stagnation cup having a drag coefficient as close to $(1 + \sigma_k)$ as can be determined experimentally. The results should be less than 1/4 % below this value due to the use of a cup having a depth of only 1/4 diameter instead of a large or infinite depth.

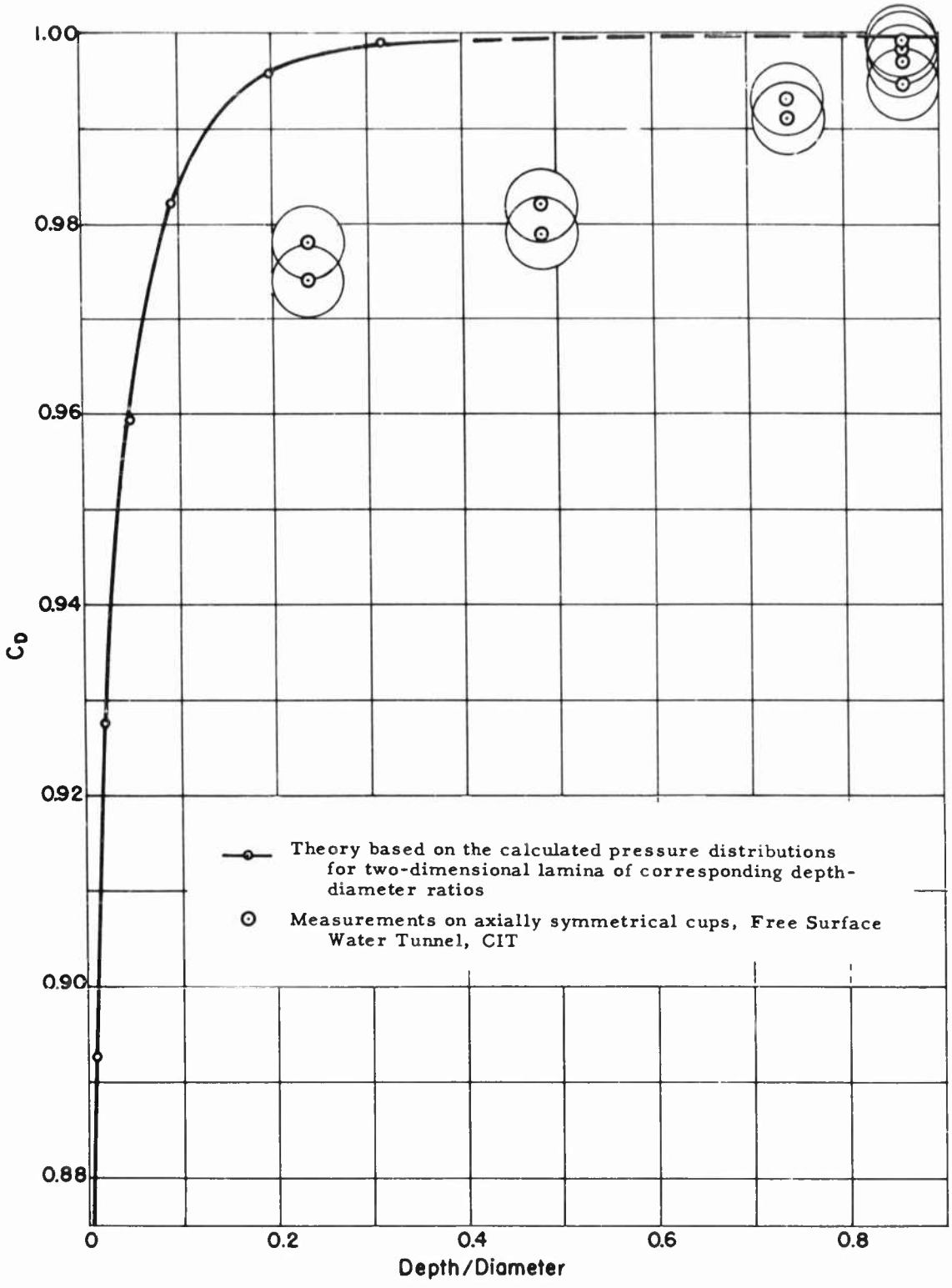

Fig. 4 - The drag coefficient of the axially symmetrical cup shown as a function of the depth-diameter ratio

The experimental agreement with the value $(1 + \sigma_k)$ is satisfactory, as shown in Fig. 2, for the usual tests on cups having a depth about equal to the diameter. When cups of reduced depth were tested during the present investigation, however, discrepancies appeared as shown in Fig. 4. The experimental values were reduced to C_{D0} by dividing by $(1 + \sigma_k)$ and then averaged to obtain the points plotted. There were from 4 to 17 measurements in the groups averaged and the group standard deviation (Hoel[10]) based on all groups measured, was 0.0038. The measured drag coefficients for the 1/4-diameter cup are five or six standard deviations below the minimum theory line. Further work would be required to establish the reason for this difference.

The group standard deviation of 0.38% indicates remarkable consistency of measurement, since it was obtained while varying the cavity parameter through a wide range. The small group standard deviation is, therefore, an indication that the data conforms with the relation $C_D = C_{D0}(1 + \sigma_k)$.

A more sensitive experimental comparison with theory was made by measuring the pressure difference between the central stagnation point and at a point midway out toward the wall at the bottom of cups of different depth-diameter ratio. As shown in Fig. 5, the experimental values of the pressure coefficient at this midpoint lie close to and slightly above the corresponding points in two-dimensional theory. This is believed sufficient evidence to justify the use of the three-dimensional theory derived from two-dimensional pressure distributions as a means of selecting a sufficient depth for a stagnation-cup calibrator. The drag coefficient measurements that appear too low in Fig. 4 indicate either an unknown source of error or the action of phenomena not yet brought into consideration.

Real fluid effects are immediately thought of as a possible reason for the drag measurements being lower than predicted by potential flow theory. This was not the case, however, since a calculation of the forward-acting surface tension force due to stretching the free surface near the cup lip and a rough-over estimation of the forward-acting shear force on the cup wall did not account for the discrepancies of Fig. 4. Furthermore, it might be expected that such forward-acting forces on the cup are partially compensated for by an increased bottom pressure brought about by the retarded circulation that they cause. The measurements in Fig. 5 that are

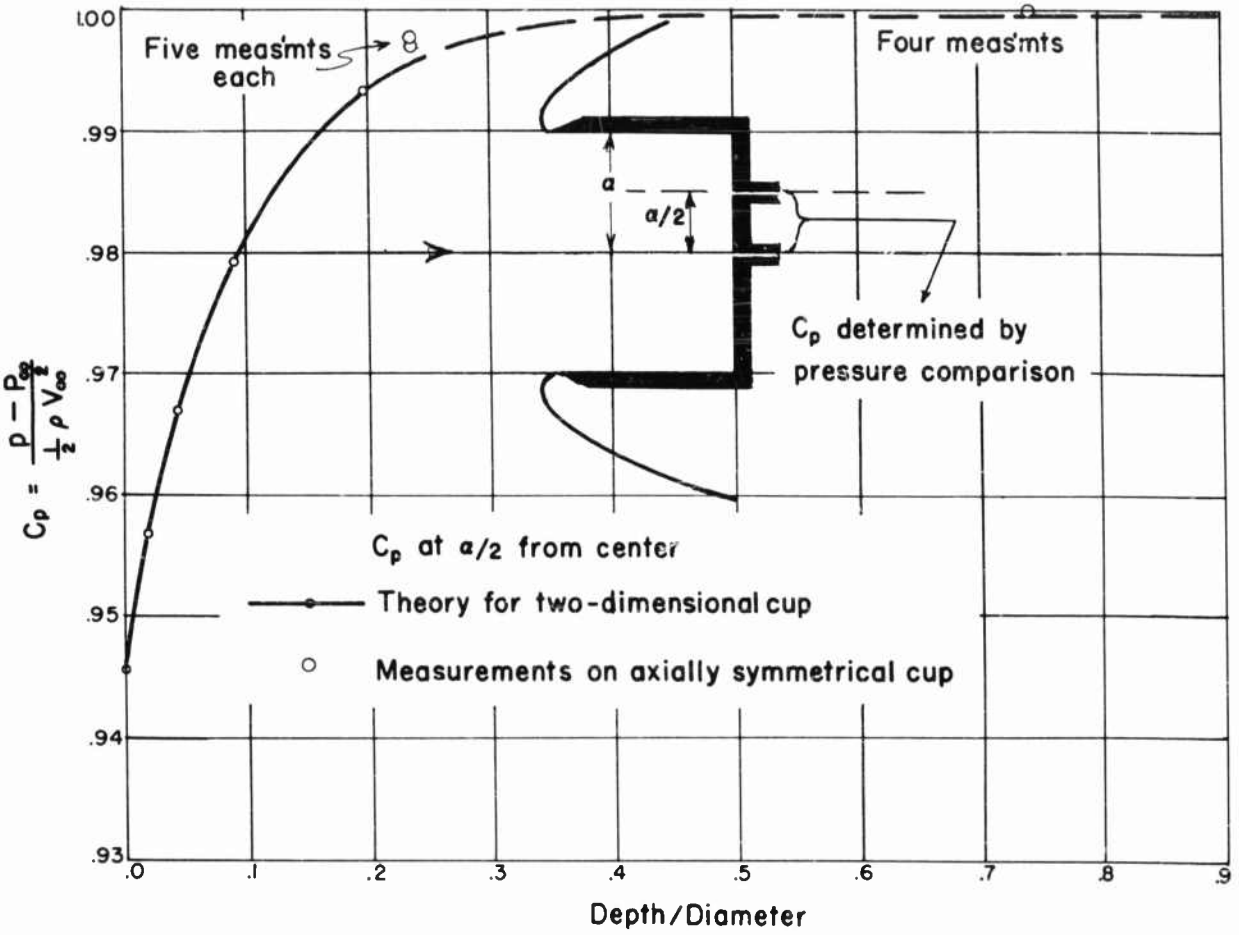

Fig. 5 - The pressure coefficient as a function of the depth-diameter ratio at a point midway out from the center of an axially symmetrical cup or a cup-shaped lamina

slightly higher than theory might be due to this effect or to the shift that is expected to be in the same direction because of differences between two- and three-dimensional flow.

Cavity Models in Theory and Experiment

In the early considerations of cavity flow by Helmholtz, Kirchhoff, Rayleigh, and others[11], zero cavity number was assumed. Under such conditions, the velocity of the cavity boundary would be equal to the velocity of the undisturbed stream, as shown by Eq. (7). Since this condition of $\sigma_k = 0$ resulted from an assumption that the pressure in the cavity was equal to the surrounding pressure p_∞, it might be expected that a stream filament deflected aside by an obstacle would never return to the line of its original path. The cavity would, therefore, extend behind an obstacle to infinity for the case of zero cavity number where there is no pressure difference, $p_\infty - p_k$, acting in a direction to return the deflected boundary toward its original path.

When there is a pressure difference, $p_\infty - p_k$, which results in a positive cavity number, the cavity boundary streamlines will return to form a finite closed cavity. Riabouchinsky,[12, 13, 14] in 1920, made the first calculation of the drag on a plate at the head of such closed cavities at $\sigma_k > 0$ by using a cavity model in which an image plate is assumed at the downstream end opposite the real plate. The free streamlines run from the edge of the real plate to the edge of the image plate. The Riabouchinsky image-body cavity model was also used by Weinig (1932)[15], by Zoller (1943)[16], and by Plesset and Shaffer in the extensive computations previously mentioned.

Image bodies or other closure bodies are not usually present when an object opens up a cavity in a fluid. Nevertheless, the pressure difference, $p_\infty - p_k$, that exists when there is a positive cavity number causes the boundary streamlines to close and form a finite cavity. It was shown by Eq. (7) that the cavity boundary streamline has a velocity greater than the free-stream velocity. Since one could only expect that the velocity decreases monotonously from V_k at the cavity wall to V_∞ at a great distance from the cavity, the velocity of the boundary streamlines is greater than that of any of the surrounding flow. With the curvature inward in the region under

consideration, this obviously requires the boundary of a closed axially or two-dimensionally symmetrical cavity to fold back into its interior. A re-entrant jet is thus formed which flows upstream into the cavity with a surface velocity $V_k = V_\infty(1 + \sigma_k)^{1/2}$ relative to the cavity-producing body. For slim cavities at low cavity numbers, the entire profile of the jet will approach this velocity since the jet is surrounded by constant pressure and, therefore, will approach constant pressure and velocity throughout.

The re-entrant jet representation of the finite cavity was used by Kriesel (1946)[17] and attributed to Prandtl's discussion in August 1945, and to indirect evidence of his proof, as early as 1929, of zero drag on the object if the back pressure of the jet is counted. Gilbarg and Rock (1946)[18] attributed the re-entrant jet representation to Wagner; Gurevitch (1946)[19] attributed it to Effros (1946)[20]. In order to get a nonzero drag for cavity numbers above zero, these investigations have excluded the action of the jet on the grounds that it is dissipated at the rear end of the cavity without affecting the forward part.

Comparisons of the calculations based on the Riabouchinsky image-plate model and the re-entrant jet configuration were made by Gilbarg and Roch, Gurevich, Wehausen[21] and Arnoff (1950)[22]. The agreement is within a fraction of a percent on the drag coefficient and cavity diameter for σ_k less than one, and on cavity length for σ_k less than about 0.4. It would seem that any difference between Plesset and Shaffer's calculation and the true drag of cones at the head of axially symmetrical cavities is due to the use of the pressure distribution for the two-dimensional case and not to the use of the Riabouchinsky image-plate model rather than the re-entrant jet model that more accurately represents the usual cavity closure.

Figure 6 is a photograph of an open cavity in the Free-Surface Water Tunnel. The re-entrant jet is seen to be tumbling forward to form a roller that dissipates the energy of the jet. The jet is not as clean as the mathematical model since it drops under the action of gravity and strikes the bottom wall of the cavity. Furthermore, in mixing with the cavity wall, it disturbs its own formation. There will be closer agreement between descriptions of open cavities by different investigators when consideration is given to the gravitational effect as determined by the Froude number and to the manner in which the re-entrant jet liquid contacts the boundaries of

the cavity. During an early part of the present investigation, the effects of changes in the Froude number on the character of the cavity and on the entrainment of cavity gas were determined[23].

The Jet Cavity as a Model of the Cavity with Re-entrant Jet

It is difficult to arrange equipment in which a clear re-entrant jet can be observed, since the jet will usually strike the cavity walls and disturb its own formation. Attempts were made to catch the frothy roller shown in Fig. 6 and pump it off through a streamlined strut, and thereby clear away the disturbance to the cavity wall so that a clear re-entrant jet could be formed. Although these attempts were unsuccessful, it is believed that some such system could be operated satisfactorily when the difficulties of establishing and stabilizing the desired steady-state conditions are overcome.

The conception of a model of the cavity with re-entrant jet, in which all streamlines have the same relative magnitude but are reversed in direction, was found to be very easily produced in the water tunnel. This is done without reversing the flow in the tunnel simply by directing a water jet upstream, as shown in Fig. 7. Similarity is maintained for any cavity number σ_k by maintaining a jet velocity $V_j = V_\infty(1 + \sigma_k)^{1/2}$. An open cavity around such a liquid jet will have its own re-entrant jet, but this can be prevented from interfering at the front end of the cavity either by a barrier or by operation at a Froude number sufficiently low that the action of gravity on the re-entrant jet will prevent it from progressing too far forward. Various points in the forward region of the flow pattern around a jet cavity will then have velocities of the same magnitude but of opposite relative direction as compared with the corresponding points in the after region of a finite symmetrical cavity having an undistrubed re-entrant jet.

The finite symmetrical cavity having an undisturbed re-entrant jet and its jet-cavity model are represented in idealized form in the diagrams of Fig. 8. The jet cavity has a Riabouchinsky type closure plate behind which the jet liquid proceeds asymptotically to V_∞, thus making it an exact model of the plate-produced cavity having an undisturbed re-entrant jet.

Fig. 6 - The re-entrant jet is projected forward from the downstream end of an open cavity

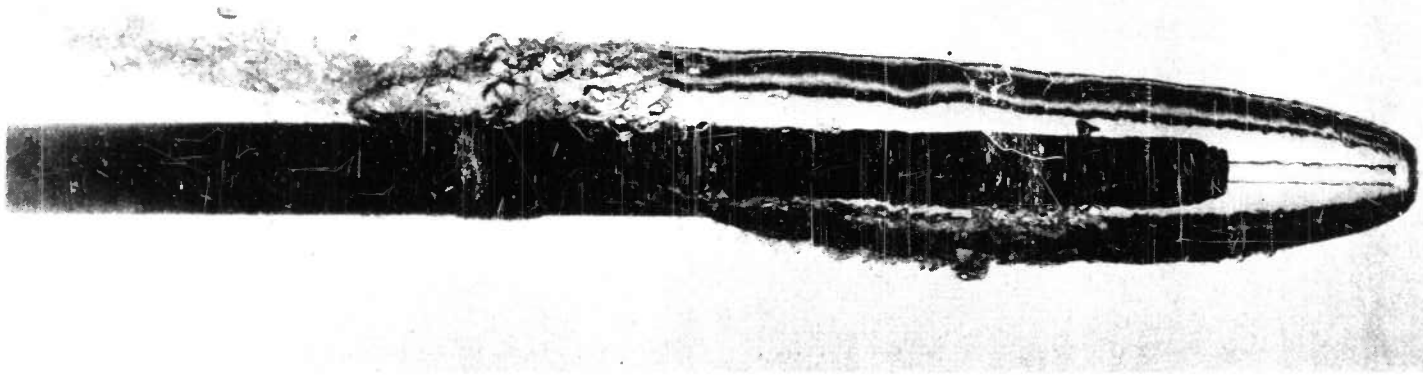

Fig. 7 - The jet cavity, a model of the cavity with re-entrant jet, is produced by directing a jet upstream in the Free-Surface Water Tunnel

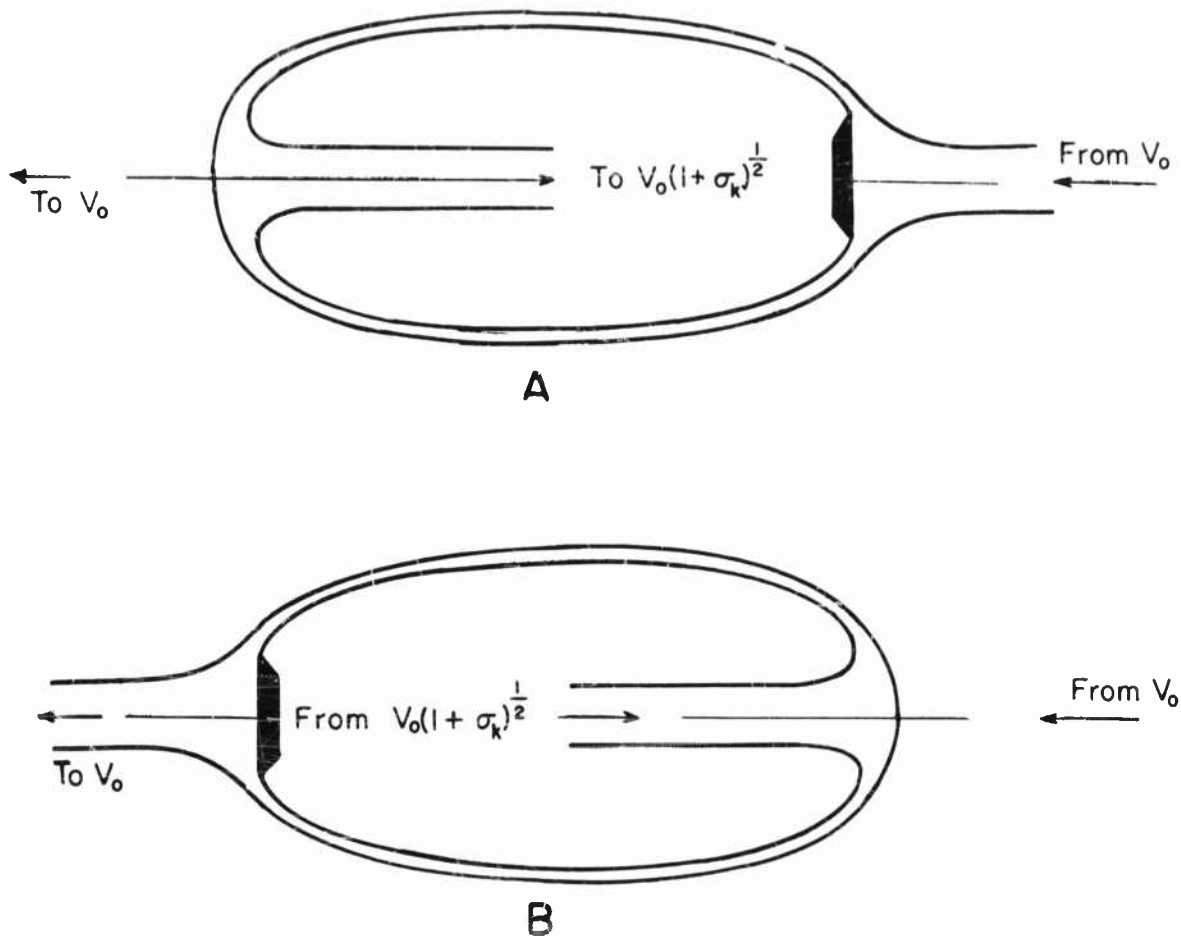

Fig. 8 - A, The symmetrical, plate-produced cavity having an undisturbed re-entrant jet, and its exact model, B, the jet cavity having a Riabouchinsky-type closure plate

The drag of the plate-produced cavity is calculated or measured with the assumption or provision that the re-entrant jet does not strike the plate. With a similar exclusion of the force on the closure plate, a calculation can be made of the drag of the jet cavity. From momentum considerations, the force required to deflect the jet in the opposite direction, i.e., the drag of the jet cavity is

$$D_j = Q \rho \Delta V \tag{12}$$

where Q is the volume rate of flow of the jet liquid of density ρ and ΔV is the change in velocity of the jet liquid in being reversed from an upstream velocity $V_j = V_\infty(1 + \sigma_k)^{1/2}$ to a downstream velocity V_∞. Since $Q = A_j V_\infty(1 + \sigma_k)^{1/2}$ where A_j is the area of the jet having a uniform velocity $V_\infty(1 + \sigma_k)^{1/2}$ and $\Delta V = V_\infty(1 + \sigma_k)^{1/2} + V_\infty$ the jet-cavity drag is

$$\begin{aligned} D_j &= \rho A_j V_\infty(1 + \sigma_k)^{1/2} \left[V_\infty(1 + \sigma_k)^{1/2} + V_\infty \right] \\ &= \rho A_j V_\infty(1 + \sigma_k) + \rho A_j V_\infty^2(1 + \sigma_k)^{1/2} \\ &= \rho A_j V_\infty^2 \left[(1 + \sigma_k) + (1 + \sigma_k)^{1/2} \right] . \end{aligned} \tag{13}$$

The drag coefficient based on the jet area A_j is

$$C_{Dj} = \frac{D_j}{q A_j} = 2 \left[(1 + \sigma_k) + (1 + \sigma_k)^{1/2} \right] \tag{14}$$

which, at small values of σ_k where $(1 + \sigma_k)^{1/2} \backsimeq 1 + \frac{1}{2} \sigma_k$, reduces to the close approximation

$$C_{Dj} \backsimeq 4 + 3 \sigma_k . \tag{14'}$$

Since the jet cavity with a closure body is a model of a cavity and re-entrant jet produced by an identical body, the drag force D_j for the jet cavity is the same as the drag D on the cavity-producing body. By substituting D_j from Eq. (13) in Eq. (8) it is seen that the drag coefficient of any body can be expressed as

$$C_D = 2 \left[(1 + \sigma_k) + (1 + \sigma_k)^{1/2} \right] \frac{A_j}{A_D} , \tag{15}$$

a result also obtained by Birkhoff[24]. Again, to a close approximation, this reduces to

$$C_D \approx \frac{A_j}{A_D}(4 + 3\,\sigma_k) \tag{15'}$$

The ratio of the separation area of a cavity-producing object to the area of the re-entrant jet is, therefore

$$\frac{A_j}{A_D} = \frac{C_D}{2\left[(1 + \sigma_k) + (1 + \sigma_k)^{1/2}\right]} \tag{16}$$

which, at small values of σ_k, becomes approximately

$$\frac{A_j}{A_D} \approx \frac{C_D}{4 + 3\,\sigma_k} \,. \tag{16'}$$

Instead of using the particular value of C_D corresponding to the value of σ_k, recourse to Eq. (11) allows the use of C_{D0}, the drag coefficient at $\sigma_k = 0$, to give the expression

$$\frac{A_j}{A_D} = \frac{C_{D0}\,(1 + \sigma_k)}{2\left[(1 + \sigma_k) + (1 + \sigma_k)^{1/2}\right]} \tag{17}$$

which is exact for a cavity produced by a stagnation cup and very close for any shape nose when σ_k is small. At small values of σ_k, however, this becomes approximately

$$\frac{A_j}{A_D} \approx \frac{C_{D0}}{4}\left(1 + \frac{1}{4}\,\sigma_k\right) . \tag{17'}$$

As a verification of the derived equations and of the similarity between the jet cavity and the cavity with re-entrant jet, measurements of jet and cavity diameter have been made at different values of the cavity number σ_k. A correction was made for the velocity distribution in the jet to determine an equivalent jet diameter for the jet cavity. The diameter of a jet having the same momentum and the velocity as dictated by the cavity pressure in accordance with Eq. (7) throughout its cross section

was determined from timed volumetric discharge measurements. The equivalent jet diameter used in making comparisons with other cavity data was 1.6% smaller than the measured nozzle exit diameter. Using these cavity and jet diameters together with the derived equations in comparison with measurements on cavities produced by other nose shapes, no significant differences are observed. This comparison requires all data to be reduced to a parameter that has a single value as a function of σ_k regardless of the nose shape producing the cavity. The jet cavity is included in the general representation of cavity characteristics presented in the following section.

The General Representation of the Drag Coefficient and the Cavity Dimensions

A drag coefficient based on the cavity diameter and defined as the cavity-drag coefficient

$$C_{Dm} \equiv \frac{D}{q A_m} , \tag{18}$$

in which A_m is the transverse area of the cavity at its maximum diameter d_m, is found to be a single valued function of the cavity parameter, regardless of the character of the obstacle producing the cavity. A representation of C_{Dm} vs. σ_k is generally applicable to all open cavities, since data for all head shapes as well as Reichardt's theory of source-sink bodies with constant pressure distribution give an identical relation.

Another useful relation, involving the separation diameter d of the object forming the cavity, makes use of the square root of the cavity-drag coefficient. From the definition equations $C_{Dm} \equiv D/(q A_m)$ and $C_D \equiv D/(q A_d)$, where C_D is based on the area A_d of the separation diameter d, it follows that

$$\sqrt{C_{Dm}} = \sqrt{C_D}\,\frac{d}{d_m} . \tag{19}$$

The diameter-length ratio of the open cavity as a function of the cavity parameter σ_k was also shown by Reichardt to agree with his theory of source-sink bodies with constant pressure distribution and to be independent of the head form producing the cavity.

The above three cavity characteristics are plotted as functions of σ_k in Fig. 9. The solid lines represent the theory of Reichardt that is based on source-sink bodies adjusted for constant pressure at the interface. Data plotted on the $\sqrt{C_D}(d/d_m)$ curve serves as a comparison for C_{Dm} since, by definition, Eq. (19) relates the two.

The theory and measurements of Reichardt agree remarkably well for the diameter-length ratio d_m/ℓ. The data for $\sqrt{C_D}(d/d_m)$ was checked roughly and extended to higher values of σ_k during the present investigation. Values of $\sqrt{C_D}(d/d_m)$ for the jet cavity are also included. They were obtained by use of the derived equations and the measured jet and cavity diameters. In support of the derived equations and the concept of the jet cavity as a model of the cavity with re-entrant jet, the agreement of this data with that of a variety of other head shapes is noted.

The cavity characteristics plotted in Fig. 9 are generally applicable to all axially symmetrical open cavities, regardless of the type of head producing them. This includes heads such as spheres and ogives where the separation boundary is not sharply defined but in all cases the diameter d is the one on which the drag coefficient C_D is based. These general cavity characteristics are related to the head shapes producing them through the use of C_D vs. σ_k curves similar to those presented in Fig. 2. For heads with an indefinite separation boundary, C_D is not necessarily a simple function of σ_k nor a function of σ_k alone. On the other hand, heads having a constant separation area as σ_k is changed will comply closely with the relation $C_D = C_{D0}(1 + \sigma_k)$. The measurements show greater slope than can be explained for the slimmer heads but the agreement improves for the blunter shapes. The agreement is within experimental error for the stagnation cup which serves as an excellent calibration device having a drag coefficient

$$C_D = 1(1 + \sigma_k).$$

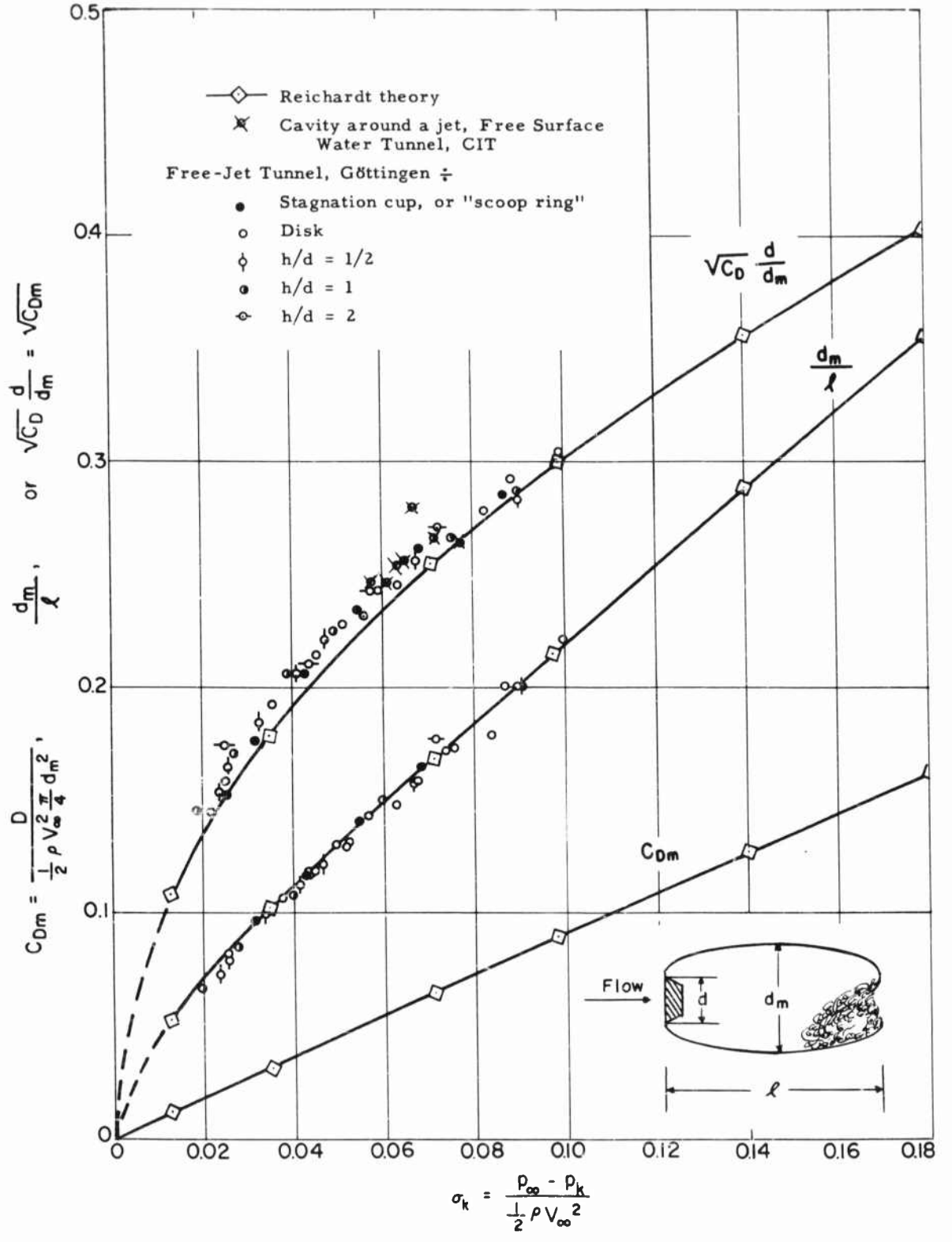

Fig. 9 - The cavity characteristics for all axially symmetrical open cavities

REFERENCES

1. Reichardt, H., "The Laws of Cavitation Bubbles at Axially Symmetrical Bodies in a Flow," translation of German Report U. M. 6628, October 1945, MAP Volkenrode, Ref: MAP-VG 69-166T, Reports and Translations No. 766, Ministry of Aircraft Production, August 1946.

2. Munzer, H. and Reichardt, H., "Rotationally Symmetrical Source-Sink Bodies with Predominately Constant Pressure Distribution", translation of German Report U. M. 6616, November 1944, Armament Research Establishment Translation No. 1/50, April 1950.

3. Plesset, Milton S. and Shaffer, Phillip A., Jr., "Drag in Cavitating Flow", Reviews of Modern Physics, Vol. 20, No. 1, pp. 228-231, January 1948.

4. Plesset, Milton S. and Shaffer, Phillip A., Jr., "Cavity Drag in Two and Three Dimensions", Journal of Applied Physics, Vol. 19, No. 10, pp. 934-939, October 1948.

5. Plesset, M. S., and Shaffer, P. A., Jr., "Cavity Drag in Two and Three Dimensions", U. S. Naval Ordnance Test Station, NavOrd Report No. 1014, Pasadena, October 1949.

6. Perry, Byrne, "Evaluation of the Integrals Occurring in the Cavity Theory of Plesset and Shaffer", Dept. of the Navy, Office of Naval Research, Contracts N6onr-24420 and 24424, Report No. 21.11, Pasadena, December 1952.

7. Eisenberg, Phillip and Pond, Hartley L., "Water Tunnel Investigations of Steady State Cavities", David W. Taylor Model Basin Report No. 668, October 1948.

8. Kermeen, R., "An Experimental Study of Vapor Cavities in a Closed-Jet Water Tunnel", Hydrodynamics Laboratory Report, California Institute of Technology (in preparation).

9. Plesset, M. S. and Perry, Byrne, "On The Application of Free Streamline Theory to Cavity Flows", Mémoires sur la Mécanique des Fluides offerts a M. D. Riabouchinsky, Publications Scientifiques et Techniques du Ministere de l'Air, Paris, 1954.

10. Hoel, P. G ., Introduction to Mathematical Statistics, John Wiley and Sons, New York, 1947.

11. Lamb, H., "Hydrodynamics", 6th ed., pp. 94-108, Cambridge University Press, 1932

12. Riabouchinsky, D., "Comptes Rendus du Congrès intern. Mathematiciens", Strassbourg, 1920.

13. Riabouchinsky, D., "Thèses presentées à la faculté des sciences de Paris", pp. 14-26 (1922).

14. Riabouchinsky, D., Proc. London Math. Soc. 25 (1926).

15. Weinig, F., "Die Ausdehnung des Kavitationsgebieten", Hydromechanische Probleme des Schiffsantriebs, Hambourg, 1932.

16. Zoller, K., "Widerstand einer ebenen Platte mit Totwassergebiet", Deutsche Luftfahrtforschung, UM 4510, August 1943.

17. Kreisel, G., "Cavitation with Finite Cavitation Numbers", Admiralty Research Laboratory, UBRC Report No. 52 R1/H/36, January 1946.

18. Gilbarg, D. and Rock, H. H., "On Two Theories of Plane Potential Flows with Finite Cavities", Naval Ordnance Laboratory Memorandum 8718, August 1946.

19. Gurevich, M. I., "Some Remarks on Stationary Schemes for Cavitation Flow about a Flat Plate", translation from Bulletin de l' Academie Des Sciences de l'URSS, Classe des Sciences Techniques 1947, No. 2, pp. 143-150 (1947), David Taylor Model Basin Translation 224, November 1948.

20. Effros, D. A., "Hydrodynamical Theory of Two-Dimensional Flow with Cavitation", Comptes Rendus (Doklady), Acad. Sci. URSS41, pp. 267-270 (1946).

21. Wehausen, J. V., "Some Remarks on Gurevich's Paper", David Taylor Model Basin Translation 224, November 1948.

22. Arnoff, Leonard E., "Re-entrant Jet Theory and Steady State Cavity Drag for Perfect Fluids", U. S. Naval Ordnance Test Station Technical Memorandum 808-37, September 1950.

23. Swanson, W. M., and O'Neill, J. P., "The Stability of an Air-Maintained Cavity Behind a Stationary Object in Flowing Water", Dept. of the Navy, Office of Naval Research, Contract N6onr-24424, Report No. M-24.3, Pasadena, September 1951.

24. Birkhoff, Garrett, "Remarks on Streamlines of Discontinuity", Revista Ci., Lima 50, 105-116 (1948).